

## Sulfide-rich metallic impact melts from chondritic parent bodies

Devin L. SCHRADER<sup>1\*</sup>, Dante S. LAURETTA<sup>1</sup>, Harold C. CONNOLLY JR.<sup>1,2,3</sup>, Yulia S. GOREVA<sup>1</sup>, Dolores H. HILL<sup>1</sup>, Ken J. DOMANIK<sup>1</sup>, Eve L. BERGER<sup>1</sup>, Hexiong YANG<sup>4</sup>, and Robert T. DOWNS<sup>4</sup>

<sup>1</sup>Lunar and Planetary Laboratory, The University of Arizona, Tucson, Arizona 85721, USA

<sup>2</sup>Department of Physical Sciences, Kingsborough Community College of the City University of New York, 2001 Oriental Blvd., Brooklyn, New York 100235, USA

<sup>3</sup>Department of Earth and Planetary Sciences, American Museum of Natural History, Central Park West, New York, New York 110024, USA

<sup>4</sup>Department of Geosciences, The University of Arizona, Tucson, Arizona 85721, USA

\*Corresponding author. E-mail: schrader@lpl.arizona.edu

(Received 11 June 2009; revision accepted 23 February 2010)

---

**Abstract**—Sacramento Wash 005 (SaW) 005, Meteorite Hills 00428 (MET) 00428, and Mount Howe 88403 (HOW) 88403 are S-rich Fe,Ni-rich metal meteorites with fine metal structures and homogeneous troilite. We compare them with the H-metal meteorite, Lewis Cliff 88432. Phase diagram analyses suggest that SaW 005, MET 00428, and HOW 88403 were liquids at temperatures above 1350 °C. Tridymite in HOW 88403 constrains formation to a high-temperature and low-pressure environment. The morphology of their metal-troilite structures may suggest that MET 00428 cooled the slowest, SaW 005 cooled faster, and HOW 88403 cooled the quickest. SaW 005 and MET 00428 contain H-chondrite like silicates, and SaW 005 contains a chondrule-bearing inclusion that is texturally and compositionally similar to H4 chondrites. The compositional and morphological similarities of SaW 005 and MET 00428 suggest that they are likely the result of impact processing on the H-chondrite parent body. SaW 005 and MET 00428 are the first recognized iron- and sulfide-rich meteorites, which formed by impact on the H-chondrite parent body, which are distinct from the IIE-iron meteorite group. The morphological and chemical differences of HOW 88403 suggest that it is not from the H-chondrite body, although it likely formed during an impact on a chondritic parent body.

---

### INTRODUCTION

Many iron meteorites contain chondrite-like silicate inclusions, suggesting their parent body was initially chondritic in composition (Benedix and McCoy 2001). Among iron meteorites, 39% of those from Antarctica are ungrouped (Wasson 1990; Weisberg et al. 2006), whereas only 15% of those outside Antarctica are ungrouped. Grouped and ungrouped iron meteorites may represent more than 50 separate parent bodies (Wasson 1990). It is possible that some of these ungrouped iron meteorites are related to each other, or to other known meteorite groups.

Large (mm cm diameter) metal- and sulfide-bearing nodules occur in ordinary chondrites. Some of them have been attributed to impact vaporization and

recondensation (Rubin 1999). The matrix of some ordinary chondrites (H and L) contains nodules which consist solely of Fe,Ni metal (Scott 1973), troilite (Rubin 1985), or mixtures of these two phases (Scott 1982; Rubin 1985). Patuxent Range (PAT) 91501, an igneous textured L chondrite impact melt, contains mm- to cm-sized metal sulfide nodules that likely formed during melting (Harvey and Roedder 1994; Mittlefehldt and Lindstrom 2001; Benedix et al. 2008). PAT 91516 and PAT 91528 are two metal-sulfide nodules that likely detached from PAT 91501 (Benedix et al. 2008). The nodule studied in Benedix et al. (2008) is 5 mm in diameter and consists of globular metal surrounded by troilite, with minor pentlandite and schreibersite at phase boundaries. PAT 91516 consists of metal regions surrounded by sinuous troilite (Clarke 1994). Similarly,

there are a small number of meteorites, such as Lewis Cliff (LEW) 88432, which are thought to be large metal nodules liberated from H chondrites and are classified as H metal (Grossman 1994). This sample set shows the ability of metal sulfide nodules to either detach from their parent meteorite in flight or weather out.

A few sulfur-rich ungrouped iron meteorites have been discovered which are likely related to the ordinary chondrites (Schrader et al. 2008; D’Orazio et al. 2009). Sahara 03505 is a sulfide-rich iron meteorite (65 g), consisting of approximately equal amounts of troilite surrounding cellular and dendritic Fe,Ni metal. Its composition and petrology suggest it formed during the impact melting of a chondritic precursor (D’Orazio et al. 2009). Due to similarities with Sahara 03505, D’Orazio et al. (2009) also suggested that the paired meteorites Roberts Massif (RBT) 04162 (52.3 g) and RBT 04299 (55.2 g) may share a similar origin.

Here we discuss the metal- and sulfide-rich meteorites Sacramento Wash (SaW) 005 (Fig. 1a), Meteorite Hills (MET) 00428 (Fig. 1b), and Mount Howe (HOW) 88403 (Fig. 1c). We compare them with each other, known iron meteorite groups, LEW 88432, Sahara 03505, RBT 04162/04299, PAT 91501/91516/91528, and metal grains from H chondrites to (1) determine whether there is a relationship between SaW 005, MET 00428, and HOW 88403; (2) determine whether they are related to known meteorites or meteorite groups; (3) determine whether they are related to a common parent body; or (4) determine whether they are related by a common formation process.

## EXPERIMENTAL PROCEDURE

We studied polished slabs of SaW 005 (sample numbers UA2006 and UA2026, henceforth split 1 and 2, respectively), MET 00428 (split 3), HOW 88403 (split 7), and LEW 88432 (split 1). These samples range in area from 20.2 to 185.8 mm<sup>2</sup> (Table 1). They were studied using optical microscopy and analyzed with the Lunar and Planetary Laboratory’s (LPL) Cameca SX-50 electron probe microanalyzer (EPMA). Interior samples of SaW 005 (42.08 and 36.07 mg), MET 00428 (78.48 mg), and HOW 88403 (39.76 mg) were analyzed using inductively coupled plasma mass spectrometry (ICP-MS) to obtain major and trace elemental bulk abundances.

We obtained backscattered electron (BSE) images and X-ray element maps (operating conditions: 15.0 kV and 40.0 nA), which provide elemental and mineralogical distributions in the samples (i.e., Figs. 2 and 3). Modal abundances of the phases were obtained using the IQmaterials<sup>®</sup> (Media Cybernetics, Inc., Bethesda, MD) program from full BSE images of each meteorite

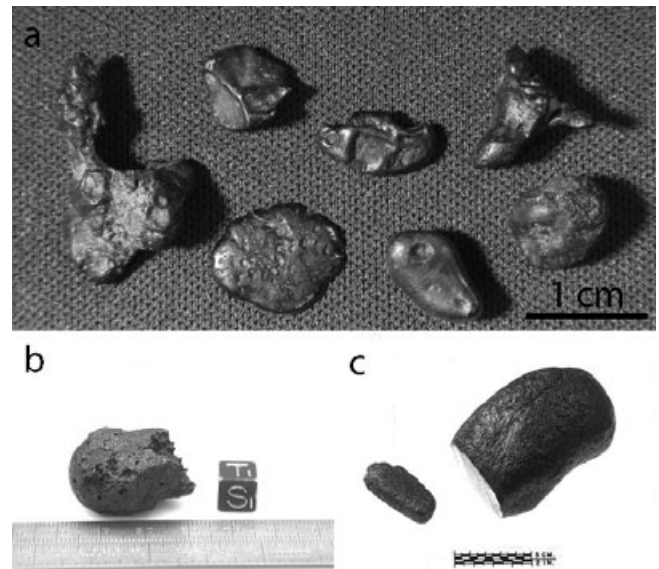


Fig. 1. Whole rock photographs of a) Sacramento Wash 005 individuals, b) MET 00428, and c) HOW 88403. a) Seven SaW 005 individuals, clockwise from far left their weights are 1.52, 0.64, 0.42, 1.19, 1.33, 0.92, and 0.45 g. On the 0.92 g piece, blue fusion crust is present, as well as rusty areas. The two pits are likely due to atmospherically excavated troilite cells; flow lines can be seen in between and around these pits. Abundant pits, likely due to atmospherically excavated troilite cells, dot the surface of the disk-shaped 0.45 g sample. b) MET 00428 (45.7774 g): the cavities on the surface of MET 00428 are likely eroded troilite cells. Cube is 1 cm on each side. c) HOW 88403 (2480.7 g) has cavities and flow lines on its surface (Clarke et al. 1990). The cavities seen on the surface are likely eroded troilite cells (i.e., Fig. 5a). Images of MET 00428 and HOW 88403 courtesy of Johnson Space Center and the Meteorite Working Group.

(Table 1). Major element abundances were characterized quantitatively by EPMA with a 1  $\mu$ m beam, both individual points and line scans, using polished and carbon-coated samples with operating conditions of 15 keV and 20 nA, a PAP correction method (a Phi-Rho-Z correction technique), and counting times of 20 s on the peak and 10 s on each background for a total of 40 s per element. Analyses were conducted using different calibration files for silicate, metal and sulfide, oxide, and phosphide analyses. Standards used for silicate analyses were albite for Na, diopside for Si, Mg, and Ca, anorthite for Al, apatite for P, orthoclase for K, rhodonite for Mn, rutile for Ti, fayalite for Fe, chromite for Cr, and nickel metal for Ni. Standards used for metal and sulfide analyses were diopside for Si, anorthite for Al, indium phosphide for P, chalcopyrite for S, chromium metal for Cr, manganese metal for Mn, titanium metal for Ti, iron metal for Fe, nickel metal for Ni, cobalt metal for Co, and chalcopyrite for Cu. Standards used for oxide

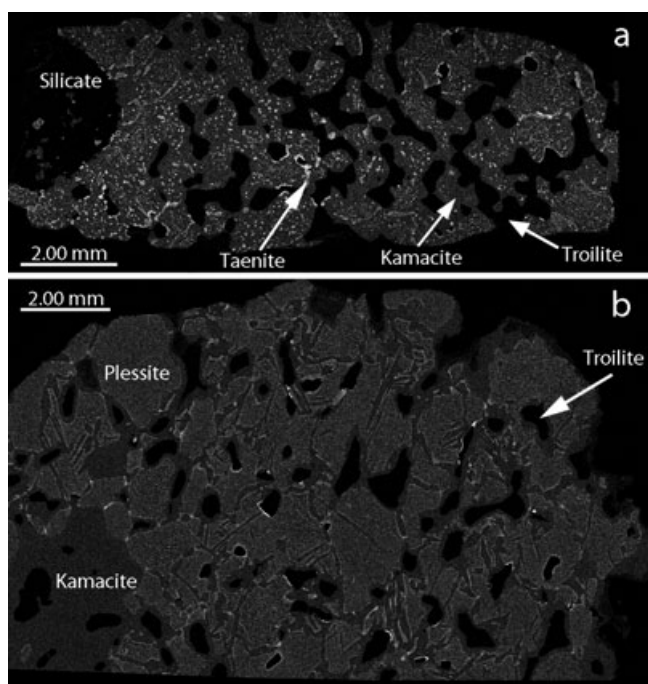


Fig. 2. Full section Ni X-ray maps of a) SaW 005 (sample UA2006) contains kamacite, taenite, and abundant troilite cells. The hemispherical dark area to the left is the silicate inclusion; b) MET 00428,3 contains kamacite lamellae, regions of plessite surrounded by taenite, and abundant troilite cells. Note the 2.0 mm scale bars.

analyses were chromite for Mg, Al, Cr, and Fe, diopside for Si and Ca, rhodonite for Mn, rutile for Ti, and nickel metal for Ni. Standards used for phosphide analyses were indium phosphide for P, chromium metal for Cr, manganese metal for Mn, titanium metal for Ti, iron metal for Fe, nickel metal for Ni, cobalt metal for Co, and chalcopyrite for Cu. EPMA detection limits are listed in Tables 2, 3, 4, and 5.

Major and trace element bulk data for SaW 005, MET 00428, and HOW 88403 were obtained by acid-dissolution ICP-MS. We determined the abundances of Fe, Ni, Co, P, S, Cr, Ge, Ga, Cu, Pt, As, Ir, Se, Mo, Os, Ru, Pd, Rh, V, W, Sb, Re, Mn, Ag, and Zn (Table 6). The ICP-MS sample solutions were prepared

Table 1. Modal abundance and cooling rates.

Sample	Area (mm <sup>2</sup> )	Sulfide %	Calc wt% S	ICP-MS wt% S	Min troilite cell width (μm)	Max troilite cell width (μm)	Max metal cell width (μm)	Min cooling rate (C s <sup>-1</sup> )
MET 00428,3	126.2	12	2.8	2.6	35.6	819.0	1852.5	0.0002
SaW 005 UA2006	66.6	26 <sup>a</sup>	6.5	3.9	65.6	714.8	1710.2	0.0002
HOW 88403,7	185.8	31	8.0	4.3	91.8	684.0	1358.6	0.0004
LEW 88432,1	20.2	Trace	–	–	–	–	–	–

MET 00428,3, 86 troilite cell widths; SaW 005 UA2006, 64 troilite cell widths; and HOW 88403,7, 155 troilite cell widths were measured.

<sup>a</sup>Ignores silicate inclusion in SaW 005.

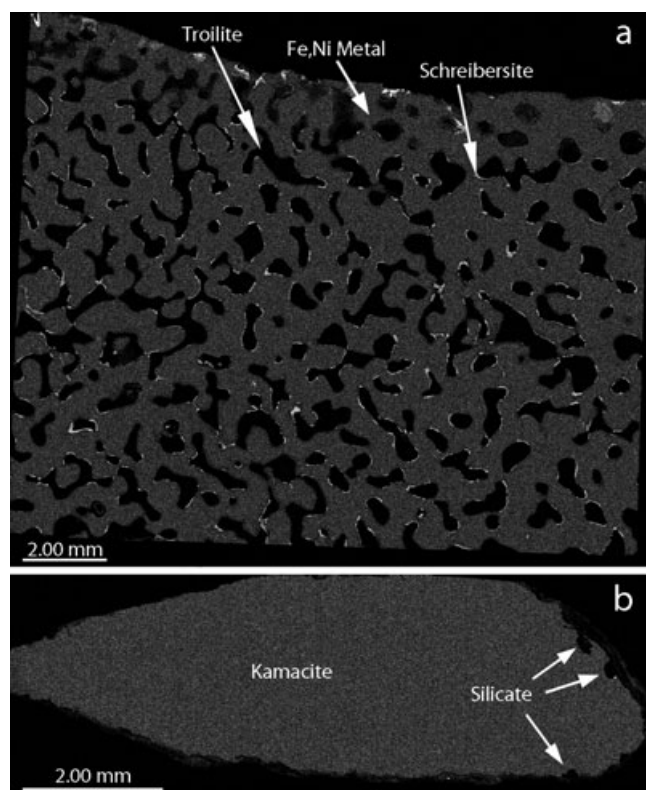


Fig. 3. Full section Ni X-ray maps of a) HOW 88403,7 contains abundant troilite cells partially surrounded by schreibersite, set in Fe,Ni metal with a plessitic structure; and b) LEW 88432,1, has a uniform texture composed of kamacite. Silicate inclusions are the dark intrusions in the upper right of the sample. Note the 2.0 mm scale bars.

by dissolving approximately 40–80 mg samples in concentrated HNO<sub>3</sub>–HCl. An analytical blank solution was prepared alongside the samples. Dissolved solutions were evaporated at 80 °C and redissolved in 5% HNO<sub>3</sub>, yielding a solution with approximately 100 μg mL<sup>-1</sup> total dissolved solids. Trace element standards consisted of known amounts of trace elements in a matrix solution containing Fe, Ni, and Co in chondritic proportions. Successive dilutions of the matrix solution alone were used as standards to quantify major

Table 2. Wt% EPMA metal and sulfide data: Sacramento Wash 005.

	S	Cr	Fe	Ni	Co	Cu	Total
<i>Host</i>							
Kamacite (107 points)							
Average	bdl	bdl	92.6	6.9	0.4	bdl	99.9
SD	bdl	bdl	1.0	0.9	0.0	bdl	0.5
Taenite (16 points)							
Average	bdl	bdl	73.8	25.8	0.1	bdl	99.8
SD	bdl	bdl	3.8	3.7	0.1	bdl	0.4
Range	bdl	bdl	69.2–83.2	17.0–31.2	bdl-0.32	bdl	–
Troilite (55 points)							
Average	36.97	bdl	63.2	bdl	bdl	bdl	100.2
SD	0.29	bdl	0.4	bdl	bdl	bdl	0.3
Copper (2 points)							
Average	0.08	bdl	2.9	0.8	bdl	97.5	101.3
SD	0.11	bdl	0.5	1.0	bdl	0.9	0.5
<i>Silicate inclusion</i>							
Kamacite (17 points)							
Average	bdl	bdl	92.4	7.5	0.4	bdl	100.3
SD	bdl	bdl	1.4	1.5	0.0	bdl	0.4
Tetrataenite (1 point)							
Average	bdl	bdl	44.7	55.5	bdl	bdl	100.2
SD	–	–	–	–	–	–	–
Troilite (14 points)							
Average	36.72	0.28	63.1	bdl	bdl	bdl	100.1
SD	0.62	0.30	0.4	bdl	bdl	bdl	0.5

Data from SaW 005 UA2006. Detection limits are 0.03 wt% for Si, 0.02 wt% for Al, 0.03 wt% for P, 0.04 wt% for S, 0.05 wt% for Cr, 0.06 wt% for Mn, 0.04 wt% for Ti, 0.11 wt% for Fe, 0.17 wt% for Ni, 0.17 wt% for Co, and 0.14 wt% for Cu. Si, Al, P, Mn, and Ti are below detection limit (bdl) in all phases.

elements. Our trace element solution standards covered six orders of magnitude ( $10 \text{ pg mL}^{-1}$  to  $1 \text{ } \mu\text{g mL}^{-1}$ ). Analyses were performed using the LPL ELEMENT2 HR-ICP-MS. Elements present at or below blank levels are reported as upper limits, defined as  $2 \times$  average blank abundances.

Raman spectroscopy of a silica inclusion in HOW 88403 was collected from an unoriented crystal at 100% power on a Thermo Almega microRaman system (Thermo Fisher Scientific, Inc., Waltham, MA), and compared against a spectral library. This system uses a solid-state laser with a wavelength of 532 nm, and a thermoelectric cooled CCD detector. The laser is partially polarized with  $4 \text{ cm}^{-1}$  resolution and a spot size of  $1 \text{ } \mu\text{m}$ .

## RESULTS

Our data allow cross-comparison between the different samples. Modal mineralogies provide important clues to the origin of each sample (Table 1). Average metal and silicate compositions were obtained by averaging all EPMA data points with totals between 99 and 101 wt%. Bulk chemical data from ICP-MS is normalized to bulk abundances in H-chondrite magnetic separates determined by radiochemical neutron activation analysis (Kong et al. 1998). SaW 005, MET

Table 3. Olivine and pyroxene compositions determined by EPMA.

	Low-calcium pyroxene							High-calcium pyroxene			
	Olivine	pyroxene				pyroxene					
	Fa	Fs	En	Wo	Fs	En	Wo				
SaW 005											
Average	18.9	15.5	83.2	1.2	11.9	68.1	20.0				
SD	0.5	1.1	1.3	0.7	4.1	15.7	19.7				
MET 00428											
Average	X	17.3	80.4	2.3	X	X	X				
SD	X	0.3	0.8	0.8	X	X	X				
LEW 88432											
Average	18.9	16.9	82.1	1.0	X	X	X				
SD	0.5	0.8	0.8	0.1	X	X	X				

X = not observed.

Equilibrated H-chondrite compositional range: olivine Fa16–20, and low-Ca pyroxene Fs14.5–18 (Brearley and Jones 1998; and references therein). SaW 005: 25 data points on olivine, 56 data points on low-Ca pyroxene, 6 high-Ca pyroxene. MET 00428: 9 pyroxene data points. LEW 88403: 15 data points on olivine, 12 on pyroxene. Detection limits are 0.04 wt% Na, 0.03 wt% Si, 0.03 wt% for Mg, 0.02 wt% for P, 0.02 wt% for Al, 0.02 wt% for K, 0.02 wt% for Ca, 0.05 wt% for Mn, 0.03 wt% for Ti, 0.13 wt% for Fe, 0.11 wt% for Cr, and 0.13 wt% for Ni.

00428, and HOW 88403 all have morphological and chemical similarities. LEW 88432 is most similar to SaW 005, but important differences are present.

Table 4. Wt% EPMA metal data: MET 00428 and HOW 88403.

	S	Cr	Fe	Ni	Co	Cu	Total
<i>MET 00428</i>							
Kamacite (66 points)							
Average	bdl	bdl	92.8	6.4	0.42	bdl	99.6
SD	bdl	bdl	1.0	1.0	0.04	bdl	0.4
Fe,Ni metal in Plessite (6 points)							
Average	bdl	bdl	84.1	15.2	0.27	bdl	99.6
SD	bdl	bdl	2.7	2.8	0.07	bdl	0.4
Range	bdl	bdl	80.8–88.3	10.5–18.2	0.19–0.39	bdl	–
Taenite (11 points)							
Average	bdl	bdl	73.0	26.5	0.16	bdl	99.7
SD	bdl	bdl	6.3	6.2	0.07	bdl	0.4
Range	bdl	bdl	61.4–78.3	21.0–38.1	bdl-0.27	bdl	–
Troilite (42 points)							
Average	36.61	bdl	63.3	bdl	bdl	bdl	99.9
SD	0.17	bdl	0.2	bdl	bdl	bdl	0.3
Copper (3 points)							
Average	0.06	bdl	1.6	1.4	bdl	98.8	101.8
SD	0.01	bdl	0.2	0.2	bdl	0.4	0.2
<i>HOW 88403</i>							
Kamacite (44 points)							
Average	bdl	bdl	91.9	7.1	0.41	bdl	99.4
SD	bdl	bdl	0.8	0.6	0.03	bdl	0.4
Fe,Ni metal in Plessite (1 point)							
Average	bdl	bdl	88.05	10.87	0.35	bdl	99.3
SD	bdl	bdl	–	–	–	bdl	–
Taenite (4 points)							
Average	bdl	bdl	76.4	23.1	0.2	bdl	99.7
SD	bdl	bdl	3.7	3.5	0.1	bdl	0.7
Range	–	–	71.1–79.4	20.2–27.7	bdl-0.25	bdl-0.20	–
Troilite (47 points)							
Average	36.58	0.18	62.7	bdl	bdl	bdl	99.4
SD	0.26	0.29	0.2	bdl	bdl	bdl	0.2

Detection limits are 0.03 wt% for Si, 0.02 wt% for Al, 0.03 wt% for P, 0.04 wt% for S, 0.05 wt% for Cr, 0.06 wt% for Mn, 0.04 wt% for Ti, 0.11 wt% for Fe, 0.17 wt% for Ni, 0.17 wt% for Co, and 0.14 wt% for Cu. Si, Al, P, Mn and Ti are below detection limit (bdl) in all phases.

Elongated and sometimes ameboid-shaped troilite grains are abundant in SaW 005, MET 00428, and HOW 88403; for simplicity, these grains will be referred to as troilite cells.

### Sacramento Wash 005

All samples of SaW 005 are found within the Franconia (H5) strewn field, in Mojave County, AZ, USA. We studied SaW 005 using two individual samples (8.60 g, SaW 005,1, and 43.7 g, SaW 005,2) from a strewn field reported to be composed of hundreds of individuals, the majority of which are <1 g. Thirteen additional samples were visually studied (ranging from 0.07 to 1.52 g), some of which have flow lines and bluish fusion crust (Fig. 1a). Half of these samples were also partially covered in caliche. Abundant cavities on the exterior of the samples appear

Table 5. Wt% EPMA metal and sulfide data: LEW 88432.

	S	Cr	Fe	Ni	Co	Total
<i>Host</i>						
Kamacite (18 points)						
Average	bdl	bdl	93.2	6.5	0.5	100.2
SD	bdl	bdl	0.3	0.1	0.1	0.4
<i>Silicate inclusion</i>						
Kamacite (2 points)						
Average	bdl	bdl	94.1	5.6	0.5	100.2
SD	bdl	bdl	0.1	0.7	0.0	0.8
Troilite (2 points)						
Average	36.43	0.08	62.8	bdl	bdl	99.3
SD	0.19	0.05	0.3	bdl	bdl	0.5

Detection limits are 0.03 wt% for Si, 0.02 wt% for Al, 0.03 wt% for P, 0.04 wt% for S, 0.05 wt% for Cr, 0.06 wt% for Mn, 0.04 wt% for Ti, 0.11 wt% for Fe, 0.17 wt% for Ni, 0.17 wt% for Co, and 0.14 wt% for Cu. Si, Al, P, Mn, and Ti are below detection limit (bdl) in all phases.

Table 6. ICP-MS major and trace element compositions, and INAA comparison.

Meteorite	WIS 91267																			
	Sacramento Wash 005			MET 00428			HOW 88403			H3.7			Jilin (H5)			Portales Valley				
	SaW 005.1	Error	005.2	Error	00428	Error	88403	Error	H3.7	Error	Bulk metal	Bulk metal	Avg bulk H metal	Avg bulk H metal	IIIAB	Error	Bear Creek	Bella Roca	Netschaëvo	
ICP-MS	ICP-MS	ICP-MS	ICP-MS	ICP-MS	ICP-MS	ICP-MS	ICP-MS	ICP-MS	ICP-MS	INAA/RNAA	INAA/RNAA	INAA/RNAA	INAA/RNAA	INAA/RNAA	INAA/RNAA	INAA/RNAA	INAA/RNAA	INAA	INAA	
This study	This study	This study	This study	This study	This study	This study	This study	This study	This study	1	1	1	1	1	2	3	4	4	5	
Fe (wt%)	88	1	90	1	89	1	87	2	86.5	90.5	88.5	88.9	88.9	88.9	nd	nd	nd	nd	nd	nd
Ni (wt%)	7.6	0.1	6.3	0.1	6.9	0.2	7.3	0.1	8.76	8.5	8.63	10.67	10.67	10.67	8.49	9.98	10.11	10.11	8.6	8.6
Co (wt%)	0.36	0.01	0.39	0.01	0.47	0.01	0.41	0.01	0.413	0.494	0.454	0.43	0.43	0.43	0.5	0.56	0.57	0.57	0.43	0.43
P (wt%)	0.004		0.01		0.021		0.295		nd	nd	nd	nd	nd	nd	0.56	nd	nd	nd	nd	nd
S (wt%)	3.9	0.1	3.8	0.1	2.6	0.1	4.3	0.1	nd	nd	nd	nd	nd	nd	nd	2.17	2.17	2.17	nd	nd
Cr ( $\mu\text{g g}^{-1}$ )	8.6		20.7		22.0		147.2		nd	nd	nd	29	4	40	nd	nd	nd	nd	nd	nd
Ge ( $\mu\text{g g}^{-1}$ )	39	2	60	2	50	2	46	1	60	123	91.5	nd	nd	38.9	32.8	30.9	30.9	30.9	66.0	66.0
Ga ( $\mu\text{g g}^{-1}$ )	20.6	0.7	17.3	0.6	14.8	0.4	19.4	0.6	9.2	12.8	11	30.4	7.6	19.7	19.1	16.7	16.7	16.7	24.8	24.8
Cu ( $\mu\text{g g}^{-1}$ )	nd		nd		213.3		284.1		346	237	291.5	nd	160	176	133	133	133	133	nd	nd
Pt ( $\mu\text{g g}^{-1}$ )	5.10		5.43		8.5		6.7		8.07	9.05	8.56	nd	nd	nd	3.40	1.70	1.70	1.70	nd	nd
As ( $\mu\text{g g}^{-1}$ )	7.4	0.2	9.2	0.3	9.1	0.3	7.3	0.4	11.9	14.2	13.05	10.0	0.5	10.5	20.8	21.2	21.2	21.2	11.6	11.6
Au ( $\mu\text{g g}^{-1}$ )	nd		nd		nd		nd		1.24	1.28	1.26	1.4	1.4	1.2	2.21	2.36	2.36	2.36	1.3	1.3
Ir ( $\mu\text{g g}^{-1}$ )	3.0	0.1	3.1	0.2	6.1	0.1	4.4	0.1	3.28	3.22	3.25	3.73	0.37	4.1	0.021	0.019	0.019	0.019	1.8-3.9	1.8-3.9
Se ( $\mu\text{g g}^{-1}$ )	nd		nd		8.00		11.56		nd	nd	nd	nd	nd	nd	nd	nd	nd	nd	nd	nd
Mo ( $\mu\text{g g}^{-1}$ )	13.6		12.8		10.1		3.0		4.48	3.96	4.22	nd	nd	7.2	nd	nd	nd	nd	nd	nd
Ru ( $\mu\text{g g}^{-1}$ )	5.58		5.26		6.32		5.72		6.50	6.65	6.58	nd	nd	nd	nd	nd	nd	nd	nd	nd
Pd ( $\mu\text{g g}^{-1}$ )	3.91		3.40		3.13		2.68		4.83	2.78	3.81	nd	nd	nd	nd	nd	nd	nd	nd	nd
Rh ( $\mu\text{g g}^{-1}$ )	1.20		1.18		1.16		1.06		1.30	0.75	1.03	nd	nd	nd	nd	nd	nd	nd	nd	nd
V ( $\mu\text{g g}^{-1}$ )	2.56		2.99		1.34		1.01		nd	nd	nd	nd	nd	nd	nd	nd	nd	nd	nd	nd
Mn ( $\mu\text{g g}^{-1}$ )	33.4		11.5		20.2		30.0		nd	nd	nd	nd	nd	nd	nd	nd	nd	nd	nd	nd
Os (ng g <sup>-1</sup> )	42		bdl		8814		5755		3580	3540	3560	nd	nd	nd	nd	nd	nd	nd	nd	nd
Sn (ng g <sup>-1</sup> )	nd		nd		nd		nd		nd	nd	nd	nd	nd	nd	nd	nd	nd	nd	nd	nd
W (ng g <sup>-1</sup> )	827		845		1146		905		616	858	737	nd	nd	1000	150	240	240	240	1200	1200
Sb (ng g <sup>-1</sup> )	173		217		284		189		505	492	498.5	nd	nd	265	nd	nd	nd	nd	nd	nd
Re (ng g <sup>-1</sup> )	291		314		721		538		352	350	351	nd	nd	nd	nd	nd	nd	nd	320	320
Ag (ng g <sup>-1</sup> )	110		bdl		561		5569		nd	nd	nd	nd	nd	nd	nd	nd	nd	nd	nd	nd
Zn (ng g <sup>-1</sup> )	88		bdl		3587		3587		nd	nd	nd	nd	nd	nd	nd	nd	nd	nd	nd	nd

Bdl = below detection limit; nd = not determined; ICP-MS = inductively coupled plasma mass spectroscopy; INAA = instrumental neutron activation analysis; RNAA = radiochemical neutron activation analysis, errors for this study are <5%, unless specifically given; 1 = data from Kong et al. (1998), errors are between 10-20% for Rh and Ge, and are <5% for all other elements; 2 = data from Ruzicka et al. (2005); 3 = data from Willis (1980); 4 = data from Willis (1980); 5 = data from Bild and Wasson (1977).

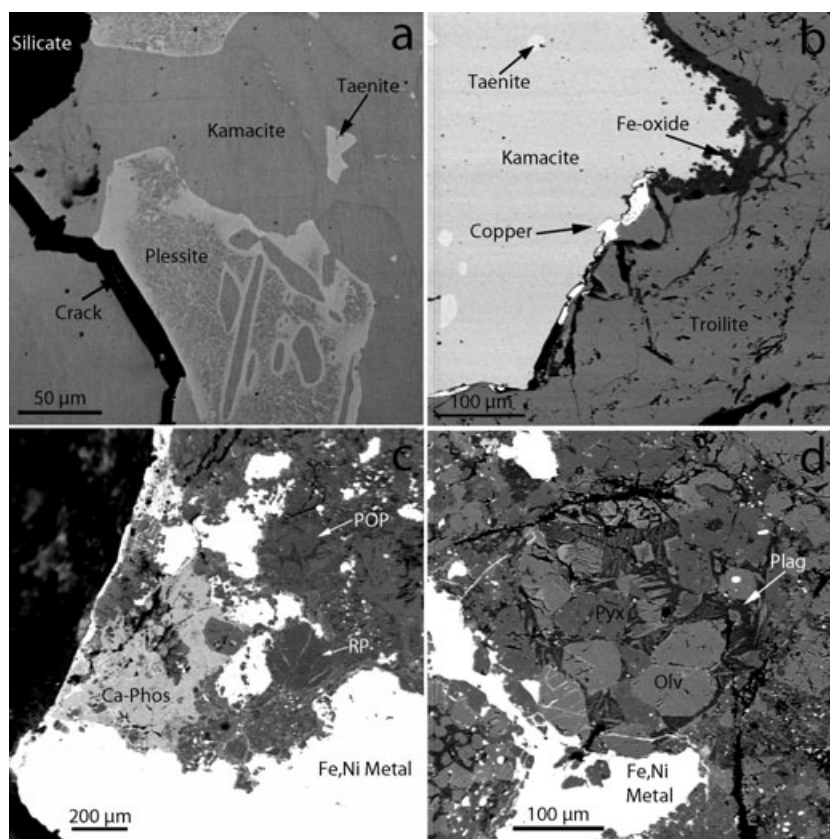


Fig. 4. BSE images of SaW 005. a) Metal region bordering the silicate inclusion consists mostly of kamacite, with taenite and plessite. A crack, likely from terrestrial weathering or sample preparation is present in the lower left. b) Edge of a troilite cell contains metallic copper along the border between troilite and kamacite. Terrestrial Fe-oxide is also present along this boundary. Taenite is present among kamacite. c) The lower left portion of the silicate inclusion shows the irregular silicate/metal interface. A large Ca-phosphate (Ca-phos) borders the Fe,Ni metal host and the silicate inclusion. Radial pyroxene (RP) and porphyritic olivine/pyroxene (POP) chondrules are visible. Large metal grains are present, at least some of which are likely protrusions into the silicate portion from the metal host. d) A POP chondrule, is approximately 250  $\mu\text{m}$  in diameter; which is consistent with the size range for H chondrites. A PO chondrule is visible in the lower left.

to be the remains of ablated and/or eroded troilite cells (Fig. 1a). The total known weight (TKW) is officially 52.3 g with main mass of 43.7 g. However, our observations of additional samples and reports from meteorite hunters suggest that the TKW is a minimum of 280 g, and is likely as high as 1000 g. We initially classified this meteorite as an ungrouped, sulfide-rich iron with affinities to the H chondrites (Connolly et al. 2008).

SaW 005,1 contains Fe,Ni metal, troilite, metallic copper, chromite, Ca-phosphate, iron oxide, and a copper-iron-sulfide (Table 2, Figs. 2a and 4). A silicate inclusion within the sample has chondrules, and contains kamacite, tetrataenite, troilite, olivine, pyroxene, plagioclase, and Ca-phosphate (Table 2, 3; Figs. 4c and 4d). SaW 005,2 is compositionally and morphologically identical to SaW 005,1 except that it does not contain chondrule bearing silicate inclusions.

The silicate portion of the meteorite comprises 9% of the cross-sectional surface area of the sample, troilite comprises 24%, and Fe,Ni metal comprises 67%. Excluding the silicate inclusion, troilite cells comprise approximately 26% of the cross-sectional surface area of the sample, with Fe,Ni metal comprising 74% (Table 1). Optical microscopy in reflected polarized light reveals that the troilite cells display abundant multiple twinning, which is likely from shock deformation (Heymann et al. 1966; Buchwald 1975; Scott 1982; Bennett and McSween 1996). Some troilite cells show abundant parallel twinning, whereas some twins are perpendicular and angled to one another.

Kamacite is the dominant phase in the meteorite, present as exsolution in taenite (Figs. 4a and 4b). Taenite surrounds regions of plessite (Figs. 2a and 4a); taenite has a Ni gradient, which ranges from 17.0 to 31.2 wt% Ni (Table 2). Troilite is present as elongated

cells in the Fe,Ni metal; their apparent long axes range from approximately 0.1 to 2.0 mm (Fig. 2a). Troilite cells display a very weak alignment from the upper left to lower right of Fig. 2a. An Fe-oxide phase, likely terrestrial oxide, surrounds portions of the troilite cells (Fig. 4b). Ca-phosphates are present as subhedral and rounded inclusions in the troilite and kamacite. Rare metallic copper is present between the Fe,Ni metal and the troilite cells (Fig. 4b). The chromites are present as euhedral and anhedral inclusions in the kamacite.

The silicate inclusion is on the edge of the sample, with apparent dimensions of  $1.7 \times 2.3$  mm (Table 3; Figs. 4c and 4d). The boundary of the silicate with the Fe,Ni metal host is irregular and silicate blebs are interspersed in the Fe,Ni metal near the boundary (Fig. 4c). The chondrule types observed are predominantly porphyritic olivine/pyroxene, but radial pyroxene is also present (Figs. 4c and 4d). All chondrules have sharp boundaries and the chondrules range in apparent diameter from 0.13 to 0.35 mm. According to the classification scheme of Van Schmus and Wood (1967) and its composition, the silicate inclusion is consistent with an H4 chondrite (Table 3).

#### **MET 00428**

This meteorite was found in two pieces that apparently broke apart during atmospheric entry, MET 00428 and MET 001038, with a TKW of 49.468 g (45.774 g and 3.694 g, respectively). It is classified as an ungrouped iron (Russell et al. 2002). Images of the whole meteorite reveal cavities, which may be the result of ablated and/or eroded troilite cells (Fig. 1b).

The meteorite contains kamacite, taenite, metallic copper, troilite, calcium-phosphate, and pyroxene (Table 3 and 4). Kamacite is the dominant phase of the meteorite, which is present as exsolution among taenite (Figs. 2b, 5a, 5b, and 5c). Kamacite lamellae range in width from approximately 100 to 120  $\mu\text{m}$  (Russell et al. 2002). The majority of kamacite is present as swathing kamacite around troilite cells (Fig. 2b). Taenite surrounds regions of plessite (Figs. 5a and 5b). Troilite is present as elongated cells within the Fe,Ni metal, their apparent long axes range from approximately 0.1 to 1.5 mm and they show a weak alignment from the upper right to the lower left of Fig. 2b. Troilite cells display abundant multiple twinning (parallel, perpendicular, and angles to one another), consistent with Russell et al. (2002). This twinning is likely from shock deformation (Heymann et al. 1966; Buchwald 1975; Scott 1982; Bennett and McSween 1996). The troilite cells comprise approximately 12% of the cross-sectional surface area of the sample, with Fe,Ni metal comprising 88%. Metallic copper is present as a small,

irregular grain with apparent dimensions of approximately  $34 \times 129$   $\mu\text{m}$ , on the edge of a troilite cell but in contact with the Fe,Ni metal (Fig. 5b). There are three small (approximately 20–40  $\mu\text{m}$  in apparent diameter) rounded and chemically equilibrated pyroxene inclusions associated with troilite cells, one of which borders kamacite (Fig. 5c). A 200  $\mu\text{m}$ , subrounded Ca-phosphate grain borders both kamacite and troilite.

#### **HOW 88403**

This meteorite was found as one single mass, with a TKW of 2480.7 g. It is classified as an ungrouped iron, and is described as an anomalous ataxite (Clarke et al. 1990; Grossman 1994). Images of the whole meteorite reveal cavities and flow lines (Clarke et al. 1990). The cavities may be from ablated and/or eroded troilite cells (Fig. 1c).

The meteorite contains kamacite, taenite, troilite, schreibersite, chromite, and the silica polymorph tridymite (Table 4). Troilite is present as elongated cells within the Fe,Ni metal, their apparent long axes range from approximately 0.10 to 2.25 mm, and show a weak alignment from the upper left to lower right of Fig. 3a. There is twinning in the troilite cells. This twinning is not present in every troilite cell, and is likely from shock deformation (Heymann et al. 1966; Buchwald 1975; Scott 1982; Bennett and McSween 1996). The troilite cells comprise approximately 31% of the cross-sectional surface area of the sample, with Fe,Ni metal comprising 69%. Schreibersite almost completely surrounds the troilite cells, the majority of which is also surrounded by swathing kamacite (Figs. 5d and 5e). Kamacite is the dominant phase of the meteorite, and is present as exsolution in a submicron intergrowth with taenite (Figs. 5d, 5e, and 5f). The bulk Ni content of HOW 88403 (approximately 7.3 wt% Ni; Table 6) places it well below the typical range for ataxites ( $\geq 15$  wt% Ni; Mittlefehldt et al. 1998). The submicron intergrowth of low- and high-Ni metal suggests HOW 88403 is best described as plessitic.

A silica inclusion, free of minor elements, is surrounded by chromite and troilite, which itself is surrounded by a discontinuous rim of schreibersite and then by swathing kamacite (Fig. 5e). Raman spectroscopy of the silica inclusion shows it to be monoclinic tridymite (Fig. 6), and its spectrum is very similar to that given by Hirose et al. (2005). One euhedral chromite grain is present in kamacite (Fig. 5f). These observations are consistent with previous work on this sample (Clarke et al. 1990), except they report the presence of phosphates. The presence of chromites, phosphates, phosphides, and its fine-grained structure suggest that the sample rapidly cooled under both

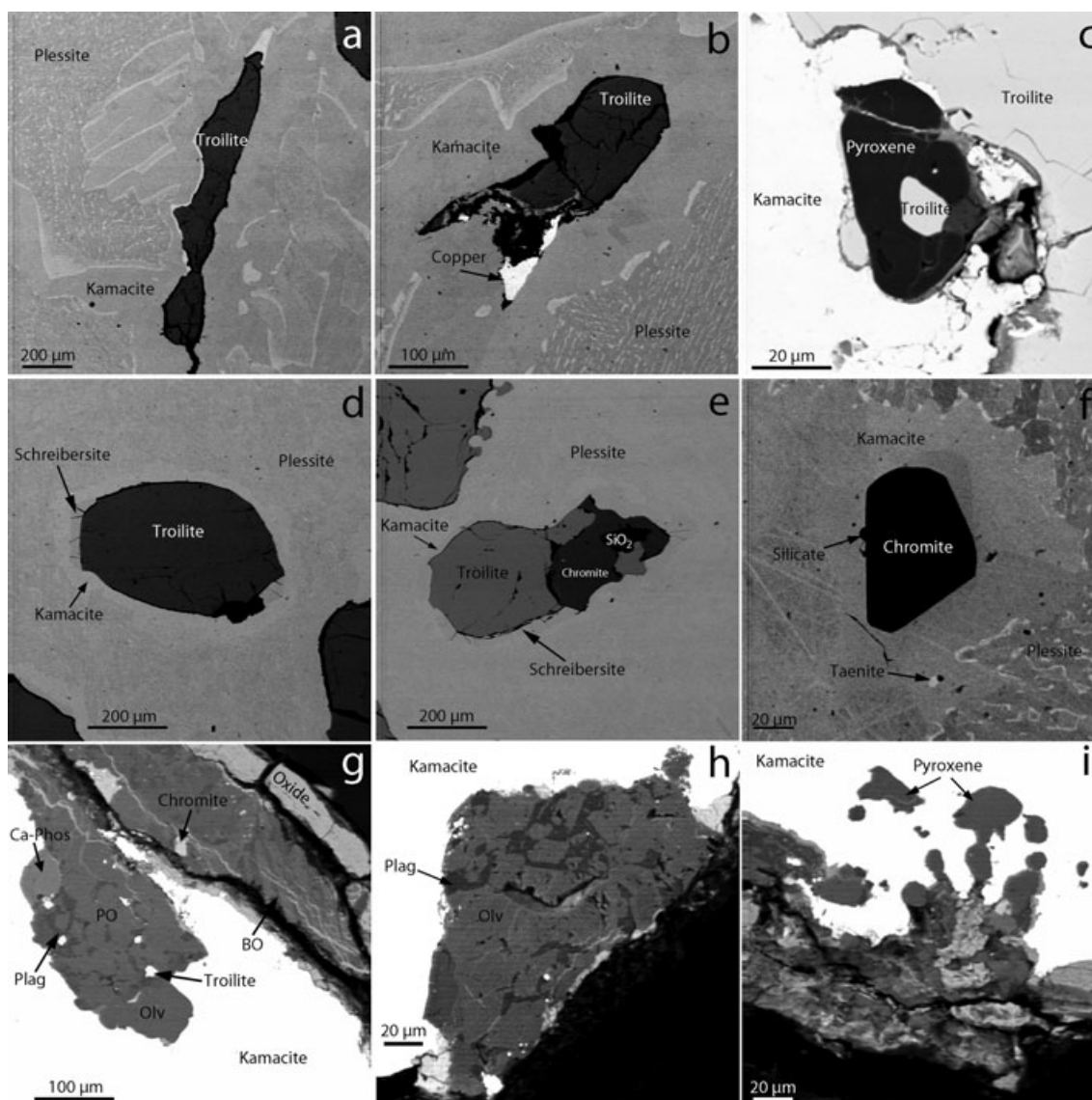


Fig. 5. BSE images of (a, b, c) MET 00428, (d, e, f) HOW 88403, and (g, h, i) LEW 88432. a) MET 00428: elongated troilite cell surrounded by swathing kamacite and plessite. b) MET 00428: metallic copper along the boundary of a troilite cell and kamacite. Swathing kamacite surrounds the troilite cell, which is surrounded by plessite. Area to the upper left of the copper grain is a hole. c) MET 00428 contains a small,  $30 \times 40 \mu\text{m}$ , rounded homogeneous pyroxene inclusion bordering troilite and kamacite. Troilite is also in its center. d) HOW 88403: troilite cell partially surrounded by schreibersite, and then by swathing kamacite, set in plessite. e) HOW 88403 contains a tridymite inclusion ( $\text{SiO}_2$ ) surrounded by chromite, surrounded by troilite, which is surrounded by schreibersite, and then by swathing kamacite set in plessite. f) HOW 88403: small chromite inclusion with a rounded silicate along the chromite/kamacite boundary. The chromite is surrounded by swathing kamacite, and by plessite. Taenite is also present. g) LEW 88432: edge of the sample, showing irregular boundary between silicates and kamacite. Texture is suggestive of porphyritic olivine (PO) and barred olivine chondrules, and is compositionally an H chondrite. Ca-phosphate (Ca-phos), troilite, and chromite are present in the silicate. A layer of oxide (likely terrestrial weathering) is along the exterior of the sample. Oliv = olivine, Plag = plagioclase. h) LEW 88432: another silicate inclusion along the edge of the sample with an irregular boundary, suggestive of a PO texture. i) LEW 88432: irregular grains of pyroxene surrounded by kamacite.

oxidizing and reducing conditions (Clarke et al. 1990). Wasson et al. (1998) suggested that HOW 88403 formed by shock melting and was present on its parent body as a large melt pocket.

#### LEW 88432

The meteorite was found as one piece with a TKW of 1.295 g. This meteorite is classified as H metal due to

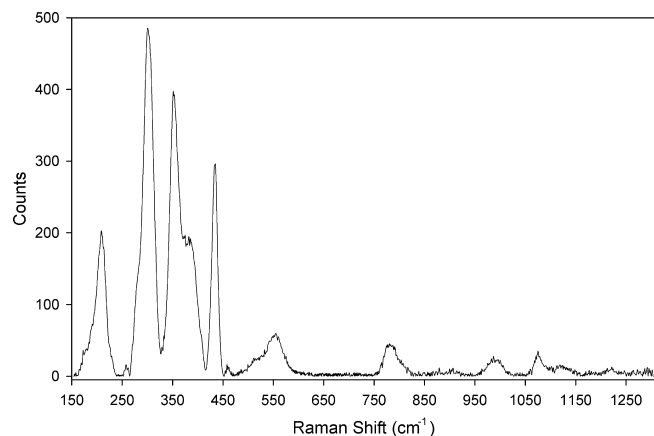


Fig. 6. Raman spectrum of monoclinic tridymite from HOW 88403 (see Fig. 5e), which is similar to that given by Hirose et al. (2005). This grain of tridymite is free of minor elements, is surrounded by chromite and troilite, which itself is surrounded by a discontinuous rim of schreibersite and then by swathing kamacite.

H-chondrite-like silicate inclusions and metal composition. Initial reports suggest that it is an Fe,Ni metal bleb from an H chondrite that passed through the atmosphere as an individual (Grossman 1994). The meteorite contains kamacite, taenite, chromite, olivine, pyroxene, troilite, and plagioclase (Tables 3 and 5). The Fe,Ni metal host is kamacite that is uniform in composition, and does not contain taenite or sulfides (Table 5; Fig. 3b). Taenite, chromite, olivine, pyroxene, troilite, and plagioclase are only present within the small silicate inclusions along the sample's edge (Figs. 3b, 5g, 5h, and 5i).

Silicate inclusions occur along the exterior of the sample, suggesting that it was at one time encased in a silicate matrix. The boundary between the metal and silicates is irregular (Figs. 5g, 5h, and 5i). The silicate inclusions are composed of olivine, pyroxene, and plagioclase, and contain small amounts of kamacite, taenite, troilite, and chromite (Tables 3 and 5). The inclusions display a variety of textures ranging from single crystals surrounded by the metal host (Fig. 5i), to inclusions reminiscent of chondritic matrix (Fig. 5g). Portions of the silicate texture suggest barred-olivine (Fig. 5g), porphyritic-olivine (Figs. 5g and 5h), and porphyritic-pyroxene chondrules, although there are no clearly defined chondrule boundaries visible. The silicate compositions are similar to those in H chondrites (Table 3).

### Major and Trace Element Compositions

The major element compositions of each sample were obtained by ICP-MS. SaW 005,1, SaW 005,2, MET 00428, and HOW 88403 are approximately

similar, with 87–90 wt% Fe, 6.3–7.6 wt% Ni, 2.6–4.3 wt% S, and 0.36–0.47 wt% Co (Table 6). MET 00428 contains the smallest amount of S, approximately 2.6 wt%, and HOW 88403 contains the largest, approximately 4.3 wt%. The wt% of S from the ICP-MS are similar to or slightly lower than the values derived from the modal abundance of S (approximately 2.8–8.0 wt%), ranging from approximately 91% to 54% of the modal values for MET 00428 and HOW 88403, respectively (Table 1). This discrepancy is most likely attributable to the heterogeneous nature of the meteorites and the small size of material analyzed. MET 00428 was the largest chip analyzed, and has the closest match between both measured S contents.

Phosphorus exhibits the largest relative difference in major element composition between the samples. HOW 88403 contains up to two orders of magnitude more P than the other samples (0.3 wt%, compared with 0.02 wt% in MET 00428 and 0.004–0.01 in SaW 005). The high P content of HOW 88403 is likely contained in its abundant schreibersite. The high P content of HOW 88403, and low abundance in MET 00428 and SaW 005 is significant because metal in chondrites typically contain significantly less P compared with iron meteorites (Herpfer et al. 1994; Yang and Goldstein 2005).

Another significant difference is the Ni content of the samples. The largest difference is between two samples of the same meteorite, SaW 005,1 and SaW 005,2 (7.6 versus 6.3 wt% Ni), suggesting sample heterogeneity at least on the size of our chips, and therefore these data may not fully represent the bulk composition of these samples (Table 6). The data for HOW 88403 agree with most values (Ga, Ge, and Ir) but differ slightly (i.e., Cr and Ni) from that presented in Wasson et al. (1998, table 2 in that paper). These small discrepancies are likely attributed to our sample containing fewer chromites than their sample (their sample had approximately 5.5× more Cr), and a lower troilite abundance.

Normalizing the major and trace element data of SaW 005, MET 00428, and HOW 88403 to the average bulk magnetic separate data for H chondrites (Kong et al. 1998), it is apparent that they share numerous similarities (Fig. 7). Trace element abundances, their similarities, and significant differences to bulk magnetic separates from H chondrites, such as Ga and Mo, are discussed in detail below.

### DISCUSSION

SaW 005 and MET 00428 are most similar in morphology and chemical composition (i.e., Figs. 1, 2, and 7; Tables 1–6). HOW 88403 shows some similarity

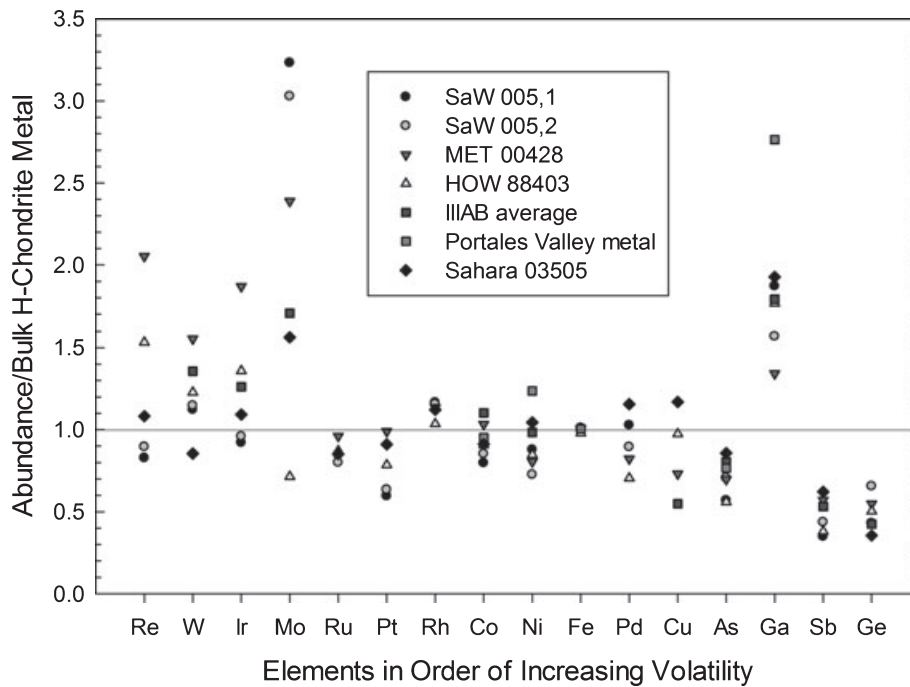


Fig. 7. Linear plot of SaW 005, MET 00428, and HOW 88403 normalized to H-chondrite magnetic separates from Kong et al. (1998) (average of Jilin [H5] and Wisconsin Range [WIS] 91267 [H3.7], by INAA/RNAA), with elements listed in increasing volatility along the X-axis. Y-axis is relative enrichment or depletion with respect to H-chondrite metal, which is represented by the straight line at a value of 1. Using ICP-MS, two samples of SaW 005 (SaW 005,1 which contained silicates, and SaW 005,2), one of MET 00428, and one of HOW 88403 were analyzed. SaW 005 was not analyzed for Cu. Average values over IIIABs from Willis (1980), Portales Valley metal data by INAA from Ruzicka et al. (2005), and Sahara 03505 data from D'Orazio et al. (2009) are plotted for reference.

to both SaW 005 and MET 00428 (i.e., taenite microstructure and the presence of cellular troilite). However, it lacks H-chondrite-like silicates, contains tridymite, and contains abundant schreibersite surrounding its sulfides. In addition, its metal structure is plessitic. The abundant schreibersite in HOW 88403 suggests that it may have formed under relatively reducing conditions compared with SaW 005 and MET 00428, which contain phosphates. LEW 88432 (H metal) shares some compositional similarities to SaW 005 and MET 00428; the kamacite compositions and silicate FeO contents are similar. Yet, unlike SaW 005 and MET 00428, LEW 88432 lacks cellular troilite and only contains taenite in its silicate inclusions.

The major and trace element compositions of SaW 005, MET 00428, and HOW 88403 share many similarities (e.g., Fe, Ni, S, Co, Ir, Ga, and Ge abundances), suggesting a possible relationship or formational process (Table 6). They show numerous similarities to bulk H-chondrite magnetic separates (Fig. 7) and plot at the low-Ni end of the IIIAB iron meteorite group, in Ni versus Ir, Ge, and Ga diagrams. However, it is important to note that the major and trace element compositions are not representative of the

metal phase, as sulfide material is included in the bulk ICP-MS samples.

### Comparison to Iron Meteorite Groups

Although S-rich iron meteorites exist, they are rare; this is partly because as the parent melt of an iron meteorite crystallizes, S is almost completely excluded (Mittlefehldt et al. 1998). Sulfide-rich meteorites are also rare because they are not as stable against collisions as iron meteorites, which have the oldest cosmic ray exposure ages of any meteorite class (Eugster et al. 2006). Compared with the iron meteorite chemical groups, SaW 005, MET 00428, and HOW 88403 are chemically closest to the IIIAB group (Table 6) (Willis 1980). Yet, the samples of this study do not have the characteristic metal morphology of the IIIABs. Also, the two S-rich IIIAB iron meteorites Bear Creek and Bella Roca (Wasson 1999) have large isolated spheroidal sulfide inclusions unlike those in SaW 005, MET 00428, and HOW 88403, and have higher Ni contents than the samples of our study. These differences suggest that these samples are not related to the IIIABs.

Iron meteorites that contain chondrite-like silicate inclusions suggest their parent-body composition was once chondritic (Benedix and McCoy 2001), such as the chondrule-bearing anomalous IIE iron Netschaëvo (Olsen and Jarosewich 1971; Bild and Wasson 1977; Mittlefehldt et al. 1998). Yet, silicate compositions and major and trace element abundances of SaW 005, MET 00428, and HOW 88403 are not similar to Netschaëvo, or other members of the IIE group (Table 6). Although SaW 005, MET 00428, and HOW 88403 are unrelated to known iron meteorite chemical groups, we are compelled to hypothesize that, because of their similarities, they may be related to each other and/or have experienced similar processes.

### Cooling Rates

The cooling rate of a Fe-Ni-S liquid will strongly determine its final structure; rapid solidification results in dendritic metal structures surrounded by troilite, whereas slower cooling rates result in a structure of cellular metal set in troilite (Blau et al. 1973; Blau and Goldstein 1975; Smith and Goldstein 1977; Scott 1982). Therefore, relative cooling rates between samples can be determined by comparing their metal structure. MET 00428 shows the most disconnected and cellular troilite, and HOW 88403 has the most connected and sinuous troilite. This variation may suggest that MET 00428 cooled the slowest, SaW 005 cooled faster, and HOW 88403 cooled the quickest. More quantitatively, the spacing between the secondary arms of the metal dendrites ( $d$ , in  $\mu\text{m}$ ) has been found to be related to the cooling rate ( $R$ , in  $^{\circ}\text{C s}^{-1}$ ) (Flemings et al. 1970; Blau et al. 1973; Flemings 1974), with the relationship given by:

$$R = 5.3 \times 10^5 \times d^{-2.9}. \quad (1)$$

Although this relationship is for the spacing of secondary arms in dendritic structures, it can be used to obtain approximate cooling rates of a cellular metal structure using metal cell widths (Blau and Goldstein 1975). As a random cross section will sample the edges of large metal cells and may make them appear smaller, a maximum cooling rate cannot be found, as measurements of the smallest metal cells are not reliable (Scott 1982). Instead, a minimum cooling rate is estimated by observing the width of the largest metal cell in each sample. Cooling rates estimated by this procedure are likely good to within a factor of 12–15 (Scott 1982). Therefore, based on maximum metal cell width the approximate minimum cooling rates for MET 00428, SaW 005, and HOW 88403 are found to be approximately  $2 \times 10^{-4}$ ,

$2 \times 10^{-4}$ , and  $4 \times 10^{-4} \text{ }^{\circ}\text{C s}^{-1}$ , respectively (Table 1). The accuracy of this technique does not allow confidence in ordering these samples by their cooling rate.

HOW 88403 is the only meteorite in this study to contain schreibersite and tridymite. The high P content, and the presence of schreibersite and tridymite could suggest that HOW 88403 does not share the same source as SaW 005 or MET 00428, and/or formed under comparatively reducing conditions. Tridymite may have formed as the result of a high degree of partial melting of a chondritic precursor, as suggested by Ulf-Møller et al. (1995) for silica in the IVA iron-meteorite group. It is also possible that the tridymite inclusion in HOW 88403 formed by oxidation of metallic Si dissolved in the liquid during cooling.

### Impact Formation on the H-Chondrite Parent Body

SaW 005 and MET 00428 are likely the result of impact-induced melting on the H-chondrite parent body. The metal and silicate compositions of SaW 005 and MET 00428 are similar to the H chondrites. They both have silicate compositions within the range for H chondrites, and inclusions in SaW 005 are chemically and morphologically identical to H4 chondrites (Table 3). The presence of metallic copper in SaW 005 and MET 00428 also suggests a relationship to the ordinary chondrites (Rubin 1994). Phosphorus is below the EPMA detection limit of 0.03 wt% in the metal phases of the meteorites of this study (Tables 2, 4, and 5), which is significant because metal in chondrites typically contain significantly less P compared with iron meteorites (Herpfer et al. 1994; Yang and Goldstein 2005), suggesting that they may be chondritic. HOW 88403's major and trace element similarities to bulk H metal suggests that it may be from a chondritic precursor, but shows enough chemical differences with SaW 005 and MET 00428 to doubt a common parent body relationship.

The main masses of SaW 005 and MET 00428 are similar, and are within the size range of large metal nodules observed in the ordinary chondrites (e.g. Scott 1973, 1982; Rubin 1985), whereas that of HOW 88403 is orders of magnitude larger. The large size of HOW 88403 (2480.7 g) suggests that it is not a plucked metal nodule from an H chondrite, but a larger melt vein or melt pocket (Wasson et al. 1998). SaW 005 was found within the Franconia (H5) strewn field and in the vicinity of seven other different H chondrites (Russell et al. 2004, 2005; Connolly et al. 2006, 2008). It is possible that SaW 005 is related to one of these meteorites, although there is currently no clear evidence to match it to any one particular sample. It is

likely that both SaW 005 and MET 00428 were at one time surrounded by H-chondrite material, but liberated early during entry through the atmosphere as some samples of SaW 005 have fusion crust and flow lines (Fig. 1a).

#### *Trace Elements*

SaW 005, MET 00428, and HOW 88403 all plot close to bulk H-chondrite magnetic separates from Kong et al. (1998) (Fig. 7). They also show similar enrichment and depletion patterns among some elements to that of Sahara 03505, which D'Orazio et al. (2009) suggests originated from impact melting of an ordinary chondrite. Relative to bulk H-chondrite data, MET 00428 is enriched in the most refractory elements; Re is enriched by 2.1 $\times$ , W by 1.6 $\times$ , and Ir by 1.9 $\times$ . HOW 88403 is also enriched in the most refractory elements, whereas SaW 005 is the closest to bulk H-chondrite metal.

The greatest deviation from bulk H-chondrite metal is in Mo with an enrichment factor up to 3.2 (Fig. 7). The large Mo variation (enriched by 2.4 $\times$  and 3.0–3.2 $\times$  for MET 00428 and SaW 005, respectively, and depleted by 0.7 $\times$  for HOW 88403) may result from variations in the oxygen fugacity under which each meteorite formed (e.g., Wark and Wasserburg 1980; Palme et al. 1982; Fegley 1985; Fegley and Palme 1985; Lauretta et al. 2009). However, the presence of phosphides in HOW 88403 compared with the presence of phosphates in SaW 005 and MET 00428 suggests that HOW 88403 is relatively reduced, whereas a Mo depletion in HOW 88403 suggests a relatively high oxygen fugacity. Therefore, the abundance of Mo is not controlled by the oxidation state. Thus, the bulk abundance of Mo is likely the result of its moderately siderophile nature (e.g., Liu and Fleet 2001).

SaW 005, MET 00428, and HOW 88403 are depleted in the volatile elements As, Sb, and Ge (depletions between 0.3 $\times$  and 0.7 $\times$ ), which suggests a temperature-controlled process, such as impact melting. The exception is that there is an enrichment in Ga across all samples, between 1.3 $\times$  and 1.9 $\times$  H-chondrite magnetic separates (Fig. 7). Gallium is likely enriched in SaW 005, MET 00428, and HOW 88403 because Ga is more lithophilic in unequilibrated ordinary chondrites, but becomes more siderophilic as petrologic type increases. Therefore, the metal component increases in Ga with increasing petrologic type whereas the silicate portion becomes depleted (Chou et al. 1973; Rambaldi and Cendales 1979). This hypothesis is further supported as the metal in Portales Valley shows an even greater enrichment in Ga with respect to bulk H-chondrite metal (2.8 $\times$ ) than our samples; no Mo data exist for additional comparison (Table 5) (data from

Ruzicka et al. 2005). Therefore, SaW 005, MET 00428, and HOW 88403 are likely from impact melting of a chondritic precursor.

#### *Morphology*

To obtain the morphology observed in SaW 005, MET 00428, and HOW 88403, peak melting temperature must have been above the Fe-FeS eutectic of 988 °C. Plotting the at% bulk data for each meteorite on a Fe-Ni-S liquidus projection diagram, we find that SaW 005, MET 00428, and HOW 88403 have liquidus temperatures above 1350 °C (Hsieh et al. 1987; Raghavan 2004); both the low S ICP-MS and higher modal S data plot in the same temperature field. The presence of tridymite in HOW 88403 further constrains a range of approximately 846–1470 °C and approximately 0–0.5 GPa for its formation, showing that during its history HOW 88403 passed through this temperature and pressure range (Tuttle and Bowen 1958; Boyd and England 1960).

As chondrule boundaries are well defined and silicates are unequilibrated in SaW 005, the temperature that the silicate experienced was likely not sustained above the peak alteration temperature for silicates of 950 °C (Brearley and Jones 1998). Therefore, the silicates appear to have been introduced, or the Fe-Ni-S liquid was mobilized to the silicates as the liquid was cooling. In contrast, the silicate inclusions in MET 00428 are rounded, chemically equilibrated, and associated with cellular troilite. Their morphology and chemistry suggest that the silicates were likely melted and coexisted with the Fe-Ni-S liquid, perhaps above 1350 °C, and crystallized during cooling.

The morphology and cooling rates of the samples suggest that the melt material must have been buried quickly after impact or never been exposed on the surface of the asteroid. Cooling at relatively shallow depth or under compacted overlying material is supported by cooling rates slow enough to form cellular troilite (instead of troilite surrounding metal dendrites), but rapid enough for troilite to not become spheroidal. The brecciated texture of SaW 005 (irregular silicate inclusion) may suggest impact and burial, whereas due to its rounded homogeneous silicate inclusions, MET 00428 was likely more thermally insulated than SaW 005 (Olsen and Jarosewich 1971; Bild and Wasson 1977; McSween 1987; Olsen et al. 1994). The presence of tridymite in HOW 88403 suggests high-temperature formation in a low-pressure environment, suggesting that it may have formed nearer to the surface than SaW 005 or MET 00428, as it might have cooled quicker than SaW 005 and MET 00428. Their chemical and morphological differences could also suggest formation by different impacts and/or local chemical variations

(i.e., different initial S contents), but almost certainly a different parent body for HOW 88403.

#### *Metal-Sulfide Nodules in Ordinary Chondrites*

Although they share some similarities, there are notable differences between SaW 005, MET 00428, and HOW 88403 to metal sulfide nodules in ordinary chondrites. In particular, the inclusions discussed in Scott (1982) have dendritic structures and cells of metal set in troilite, whereas the samples of this study have cellular troilite set in metal. Sahara 03505, likely an impact melt from either an H or L chondrite, and RBT 04162/04299 have dendritic/cellular metal structures (D’Orazio et al. 2009). PAT 91516, paired to the L-impact melt PAT 91501, consists of metal regions surrounded by sinuous troilite (Clarke 1994; Benedix et al. 2008). A metal sulfide nodule from the H4 regolith breccia Dimmitt is composed of troilite cells aligned in parallel, for which a cooling rate of  $90\text{ }^{\circ}\text{C s}^{-1}$  was estimated (Fig. 4 in Scott 1982). Scott (1982) suggested that this nodule started with a fine dendritic structure that annealed, causing the troilite blebs to form in parallel rows. Annealing may explain why this nodule has a more rapid cooling rate, but is morphologically similar to SaW 005, MET 00428, and HOW 88403.

The morphology of these metal- and sulfide-rich meteorites and nodules is correlated to their cooling rates. Sahara 03505 (D’Orazio et al. 2009) and the sulfide-rich nodules discussed in Scott (1982) have rapid cooling rates,  $1\text{--}4$  and  $1\text{--}300\text{ }^{\circ}\text{C s}^{-1}$ , respectively, which led to dendritic/cellular metal structures and cellular troilite in parallel rows. Scott (1982) suggested that these rapid cooling rates can be explained by impact formation near the parent body’s surface. In comparison, SaW 005, MET 00428, and HOW 88403 likely cooled at least four orders of magnitude slower, leading to large weakly aligned troilite cells. Their slower cooling rates suggest that they were more thermally insulated than Sahara 03505 (D’Orazio et al. 2009) and the metal sulfide inclusions in ordinary chondrites (Scott 1982).

Although morphologically distinct, LEW 88432 was included in this study to compare our samples to an H-metal meteorite. The FeO content of LEW 88432 is within the range of H chondrites, that of SaW 005 (the Fa content being identical), and is similar in composition to that in MET 00428 (Table 3). Although, LEW 88432’s host metal composition and morphology differ significantly as it is composed of homogeneous kamacite. LEW 88432’s composition and morphology suggests it is a large metal grain from an H chondrite, which did not form by the same mechanism that resulted in SaW 005 and MET 00428.

#### **Nomenclature**

D’Orazio et al. (2009) suggested the term sulfide-iron for Sahara 03505, RBT 04162/04299, SaW 005, MET 00428, and HOW 88403. The term sulfide-irons is useful to relate these unique meteorites in the same way the terms stony, stony-iron, and iron meteorite are used to put a large number of meteorite groups with unique parent bodies and formational histories under a general name. Therefore, we concur with the use of the term sulfide-iron proposed by D’Orazio et al. (2009) to refer to these meteorites, but suggest that more descriptive group names be applied once the sample set grows and parent-body relationships become apparent. To that end, SaW 005 and MET 00428 are most likely the first sulfide-iron-rich meteorites from the H-chondrite parent body.

#### **CONCLUSIONS**

There are compositional and morphological similarities between SaW 005, MET 00428, and HOW 88403, which suggests a common formation process. SaW 005 and MET 00428 have clear genetic links to the H chondrites (FeO content of silicates, and major and trace element composition). HOW 88403 is clearly more reduced than SaW 005 and MET 00428, with no clear link to H chondrites. SaW 005 and MET 00428 likely formed by impact-induced melting on the H-chondrite parent body, whereas HOW 88403 likely formed by impact melting on a different chondritic parent body. Bulk composition suggests that they were liquids above  $1350\text{ }^{\circ}\text{C}$ . Estimated cooling rates suggest that SaW 005, MET 00428, and HOW 88403 formed buried, but near the surface of their parent bodies.

SaW 005 and MET 00428 are the first sulfide-iron-rich meteorites related to the H chondrites, which are distinct from the IIE-iron meteorite group. The discovery that these meteorites, and likely others, are related to a known meteorite group decreases the number of ungrouped iron meteorites and therefore the number of parent bodies needed to explain them. These meteorites shed light on the important effect that impacts have had on the evolution of the H-chondrite parent body, and the alteration processes taking place in the solar system.

*Acknowledgments*—We thank Tim McCoy, Linda Welzenbach, Ed Scott, and Jeffery Grossman for helpful discussions. We thank Pete Myers, Jim Smaller, and JSC and MWG for samples, and Chen Li for assistance with Raman spectroscopy. We also thank Massimo D’Orazio, Tim McCoy, Joe Goldstein, and

Associate Editor Nancy Chabot for helpful comments and reviews. This research was funded in part by the Carson Fellowship at the LPL (D. L. S.), NASA Grant NNX07AF96G (D. S. L., PI), and NNG05GF39G (H. C. C. Jr., PI). This paper is dedicated to the memory of Jim Smaller.

*Editorial Handling*—Dr. Nancy Chabot

## REFERENCES

- Benedix G. K. and McCoy T. J. 2001. Constraining the formation conditions of silicate-bearing iron meteorites (abstract 3843). Eleventh Annual V. M. Goldschmidt Conference.
- Benedix G. K., Ketcham R. A., Wilson L., McCoy T. J., Bogard D. D., Garrison D. H., Herzog G. F., Xue S., Klein J., and Middleton R. 2008. The formation and chronology of the PAT 91591 impact melt L chondrite with vesicle-metal-sulfide assemblages. *Geochimica et Cosmochimica Acta* 72:2417–2428.
- Bennett M. E. III and McSween H. Y. Jr. 1996. Shock features in iron-nickel metal and troilite of L-group ordinary chondrites. *Meteoritics & Planetary Science* 31:255–264.
- Bild R. W. and Wasson J. T. 1977. Netschaëvo: A new class of chondritic meteorite. *Science* 197:58–62.
- Blau P. J. and Goldstein J. I. 1975. Investigation and simulation of metallic spherules from lunar soils. *Geochimica et Cosmochimica Acta* 39:305–324.
- Blau P. J., Axon H. J., and Goldstein J. I. 1973. Investigation of the Canyon Diablo metallic spheroids and their relationship to the breakup of the Canyon Diablo meteorite. *Journal of Geophysical Research* 78:363–374.
- Boyd F. R. and England J. L. 1960. The quartz-coesite transition. *Journal of Geophysical Research* 65:749–756.
- Brearley A. J. and Jones R. H. 1998. Chondritic meteorites. In *Planetary materials* edited by Papike J. J. Reviews in mineralogy, vol. 36., Washington: The Mineralogical Society of America. pp. 3-1–3-398.
- Buchwald V. F. 1975. *Handbook of iron meteorites*. Berkeley and Los Angeles: University of California Press.
- Chou C.-L., Baedeker P. A., and Wasson J. T. 1973. Distribution of Ni, Ga, Ge and Ir between metal and silicate portions of H-group chondrites. *Geochimica et Cosmochimica Acta* 37:2159–2171.
- Clarke R. S. Jr. 1994. PAT 91516. In *Antarctic meteorite Newsletter 17*, edited by Score R. and Lindstrom M. M. Houston, TX: NASA Johnson Space Center. pp. 15–16.
- Clarke R. S. Jr., Buchwald V. F., and Olsen E. 1990. Anomalous ataxite from Mount Howe, Antarctica. *Meteoritics* 25:354.
- Connolly H. C. Jr., Zipfel J., Grossman J. N., Folco L., Smith C., Jones R. H., Righter K., Zolensky M., Russell S. S., Benedix G., Yamaguchi A., and Cohen B. A. 2006. The Meteoritical Bulletin, no. 90. *Meteoritics & Planetary Science* 41:1383–1418.
- Connolly H. C. Jr., Smith C., Benedix G., Folco L., Righter K., Zipfel J., Yamaguchi A., and Chennaoui Aoudjehane H. 2008. The Meteoritical Bulletin, no. 93. *Meteoritics & Planetary Science* 43:573–632.
- D’Orazio M., Folco L., Chaussidon M., and Rochette P. 2009. Sahara 03505 sulfide-rich iron meteorite: Evidence for efficient segregation of sulfide-rich metallic melt during high-degree impact melting of an ordinary chondrite. *Meteoritics & Planetary Science* 44:221–231.
- Eugster O., Herzog G. F., Marti K., and Caffee M. W. 2006. Irradiation records, cosmic-ray exposure ages, and transfer times of meteorites. In *Meteorites and the early solar system II*, edited by Lauretta D. S. and McSween H. Y. Tucson, AZ: The University of Arizona Press. pp. 829–851.
- Fegley B. Jr. 1985. Oxidation state indicators for the solar nebula (abstract). 16th Lunar and Planetary Science Conference. pp. 232–233.
- Fegley B. Jr. and Palme H. 1985. Evidence for oxidizing conditions in the solar nebula from Mo and W depletions in refractory inclusions in carbonaceous chondrites. *Earth and Planetary Science Letters* 72:311–326.
- Flemings M. C. 1974. *Solidification processing*. New York: McGraw-Hill.
- Flemings M. C., Poirier D. R., Barone R. V., and Brody H. D. 1970. Microsegregation in iron-based alloys. *Journal of Iron Steel Institute* 208:371–381.
- Grossman J. N. 1994. The Meteoritical Bulletin, no. 76. The U.S. Antarctic Meteorite Collection. *Meteoritics* 29:100–143.
- Harvey R. P. and Roedder E. 1994. Melt inclusions in PAT 91501: Evidence from crystallization from an L chondrite impact melt (abstract). 25th Lunar and Planetary Science Conference. p. 513.
- Herpfer M. A., Larimer J. W., and Goldstein J. I. 1994. A comparison of metallographic cooling rate methods used in meteorites. *Geochimica et Cosmochimica Acta* 58:1353–1365.
- Heymann D., Lipshultz M. E., Nielsen B., and Anders E. 1966. Canyon Diablo meteorite: Metallographic and mass spectrometric study 56 fragments. *Journal of Geophysical Research* 71:619–641.
- Hirose T., Kihara K., Okuno M., Fujinami S., and Shinoda K. 2005. X-ray, DTA and Raman studies of monoclinic tridymite and its higher temperature orthorhombic modification with varying temperature. *Journal of Mineralogical and Petrological Sciences* 100:55–69.
- Hsieh K. C., Vlach K. D., and Chang Y. A. 1987. The Fe-Ni-S system. I. A thermodynamic analysis of the phase equilibria and calculation of the phase diagram from 1173 to 1673 K. *High Temperature Science* 23:17–38.
- Kong P., Ebihara M., and Xie X. 1998. Reevaluation of formation of metal nodules in ordinary chondrites. *Meteoritics & Planetary Science* 33:993–998.
- Lauretta D. S., Goreva J. S., Hill D. H., Killgore M., La Blue A. R., Campbell A., Greenwood R. C., Verchovsky A. B., and Franchi I. A. 2009. The Fountain Hills unique CB chondrite: Insights into thermal processing on the CB parent body. *Meteoritics & Planetary Science* 44:823–838.
- Liu M. and Fleet M. E. 2001. Partitioning of siderophile elements (W, Mo, As, Ag, Ge, Ga, and Sn) and Si in the Fe-S system and their fractionation in iron meteorites. *Geochimica et Cosmochimica Acta* 65:671–682.
- McSween H. Y. Jr. 1987. *Meteorites and their parent planets*. New York: Cambridge University Press. pp. 176–177.
- Mittlefehldt D. W. and Lindstrom M. M. 2001. Petrology and geochemistry of Patuxent Range 91501 and Lewis Cliff 88663. *Meteoritics & Planetary Science* 36:439–457.
- Mittlefehldt D. W., McCoy T. J., Goodrich C. A., and Kracher A. 1998. Non-chondritic meteorites from asteroidal bodies. In *Planetary materials* edited by Papike

- J. J. Reviews in Mineralogy, vol. 36., Washington: The Mineralogical Society of America. pp. 4-1-4-195.
- Olsen E. and Jarosewich E. 1971. Chondrules: First occurrence in an iron meteorite. *Science* 174:583-585.
- Olsen E., Davis A., Clarke R. S. Jr., Schultz L., Weber H. W., Clayton R., Mayeda T., Jarosewich E., Sylvester P., Grossman L., Wang M.-S., Lipshutz M. E., Steele I. M., and Schwade J. 1994. Watson: A new link in the IIE iron chain. *Meteoritics* 29:200-213.
- Palme H., Spettel B., and Wlotzka F. 1982. Fractionation of refractory metals in Ca, Al-rich inclusions from carbonaceous chondrites. *Meteoritics* 17:267.
- Raghavan V. 2004. Fe-Ni-S (iron-nickel-sulfur). *Journal of Phase Equilibria and Diffusion* 25:373-381.
- Rambaldi E. R. and Cendales M. 1979. Moderately volatiles siderophiles in ordinary chondrites. *Earth and Planetary Science Letters* 44:397-408.
- Rubin A. E. 1985. Impact melt products of chondritic material. *Reviews of Geophysics* 23:277-300.
- Rubin A. E. 1994. Metallic copper in ordinary chondrites. *Meteoritics* 29:93-98.
- Rubin A. E. 1999. Formation of large metal nodules in ordinary chondrites. *Journal of Geophysical Research* 104:30799-30804.
- Russell S. S., Zipfel J., Grossman J. N., and Grady M. M. 2002. The Meteoritical Bulletin, no. 86. *Meteoritics & Planetary Science* 37:A157-A184.
- Russell S. S., Folco L., Grady M. M., Zolensky M. E., Jones R., Righter K., Zipfel J., and Grossman J. N. 2004. The Meteoritical Bulletin, no. 88. *Meteoritics & Planetary Science* 39:A215-A272.
- Russell S. S., Zolensky M. E., Righter K., Folco L., Jones R., Connolly H. C. Jr., Grady M. M., Zipfel J., and Grossman J. N. 2005. The Meteoritical Bulletin, no. 89. *Meteoritics & Planetary Science* 40:A201-A263.
- Ruzicka A., Killgore M., Mittlefehldt D. W., and Fries M. D. 2005. Portales Valley: Petrology of a metallic-melt meteorite breccia. *Meteoritics & Planetary Science* 40:261-295.
- Schrader D. L., Connolly H. C. Jr., and Lauretta D. S. 2008. Sacramento Wash 005 and MET 00428: Impact generated sulfide-rich Fe,Ni melts from the H-chondrite parent body (abstract #1185). 39th Lunar and Planetary Science Conference. CD-ROM.
- Scott E. R. D. 1973. Large metal nodules in ordinary chondrites (abstract). *Eos Transactions, American Geophysical Union* 54:1125-1126.
- Scott E. R. D. 1982. Origin of rapidly solidified metal-troilite grains in chondrites and iron meteorites. *Geochimica et Cosmochimica Acta* 46:812-823.
- Smith B. A. and Goldstein J. I. 1977. The metallic microstructures and thermal histories of severely reheated chondrites. *Geochimica et Cosmochimica Acta* 41:1061-1072.
- Tuttle O. F. and Bowen N. L. 1958. Origin of granite in the light of experimental studies in the system NaAlSi<sub>3</sub>O<sub>8</sub>-SiO<sub>2</sub>-H<sub>2</sub>O. *Geological Society of America Memorandum* 74:143-145.
- Ulf-Møller F., Rasmussen K. L., Prinz M., Palme H., Spettel B., and Kallemeyn G. W. 1995. Magmatic activity on the IVA parent body: Evidence from silicate bearing iron meteorites. *Geochimica et Cosmochimica Acta* 59:4713-4723.
- Van Schmus W. R. and Wood J. A. 1967. A chemical-petrologic classification for the chondrite meteorites. *Geochimica et Cosmochimica Acta* 31:747-756.
- Wark D. A. and Wasserburg G. J. 1980. Anomalous mineral chemistry of Allende FUN inclusions C1, EK-141 and EGG 3 (abstract). 11th Lunar and Planetary Science Conference. pp. 1214.
- Wasson J. T. 1990. Ungrouped iron meteorite in Antarctica: Origin of anomalously high abundance. *Science* 249:900-902.
- Wasson J. T. 1999. Trapped melt in IIIAB irons; solid/liquid element partitioning during the fractionation of the IIIAB magma. *Geochimica et Cosmochimica Acta* 63:2875-2889.
- Wasson J. T., Choi B.-G., Jerde E. A., and Ulf-Møller F. 1998. Chemical classification of iron meteorites: XII. New members of the magmatic groups. *Geochimica et Cosmochimica Acta* 62:715-724.
- Weisberg M. K., McCoy T. J., and Krot A. N. 2006. Systematics and evaluation of meteorite classification. In *Meteorites and the early solar system II*, edited by Lauretta D. S. and McSween H. Y. Tucson: The University of Arizona Press. pp. 19-52.
- Willis J. 1980. The bulk composition of iron meteorite parent bodies. Ph.D. dissertation, University of California at Los Angeles, Los Angeles, CA, USA.
- Yang J. and Goldstein J. I. 2005. The formation of the Widmanstätten structure in meteorites. *Meteoritics & Planetary Science* 40:239-253.
-